

Large-Scale Synthesis of Transition-Metal-Doped TiO₂ Nanowires with Controllable Overpotential

Bin Liu,^{†,‡} Hao Ming Chen,^{†,‡} Chong Liu,^{†,⊥} Sean C. Andrews,^{†,⊥} Chris Hahn,[†] and Peidong Yang^{*,†,§,⊥}

[†]Department of Chemistry and [§]Department of Materials Science and Engineering, University of California, Berkeley, California 94720, United States

[⊥]Materials Sciences Division, Lawrence Berkeley National Laboratory, Berkeley, California 94720, United States

S Supporting Information

ABSTRACT: Practical implementation of one-dimensional semiconductors into devices capable of exploiting their novel properties is often hindered by low product yields, poor material quality, high production cost, or overall lack of synthetic control. Here, we show that a molten-salt flux scheme can be used to synthesize large quantities of high-quality, single-crystalline TiO₂ nanowires with controllable dimensions. Furthermore, *in situ* dopant incorporation of various transition metals allows for the tuning of optical, electrical, and catalytic properties. With this combination of control, robustness, and scalability, the molten-salt flux scheme can provide high-quality TiO₂ nanowires to satisfy a broad range of application needs from photovoltaics to photocatalysis.

Over the past two decades, tremendous effort has been directed toward the synthesis of one-dimensional (1D) materials, whose unique chemical/physical properties can potentially be exploited in various fields, including optoelectronic, photovoltaic, electrochemical, and electromechanical devices.^{1–9} Many synthetic methods have been developed for growing 1D semiconductors, including vapor–liquid–solid,^{10,11} vapor–solid,¹² solution–liquid–solid,¹³ and hydrothermal/solvothermal techniques.^{14–16} However, these methods typically trade either yield for quality or vice versa. Since the future of 1D semiconductor nanotechnology depends on the balance between materials yield and subsequent device performance,¹⁷ development of synthetic routes capable of simultaneously satisfying the needs of high yield, large-scale production, and high material quality continues to require great ingenuity. Molten-salt flux synthesis is accomplished by utilizing a mixture of molten salts as a highly reactive medium, where there is facile diffusion in the liquid state. Eutectic salt compositions are commonly utilized for maximal reactivity at their respective minimal required temperature, where the mobility of ions in these molten salts is approximately 10¹⁰ times higher than in the solid state.¹⁸ Once the product material is less soluble than the reactants in the salt solution, various salt mixtures can be tailored to the reactants and subsequent products of choice.^{19,20}

Herein, we report a molten-salt route to synthesize large quantities of high-quality, single-crystalline TiO₂ nanowires. In this technique, commercially available TiO₂ nanoparticles and common salt mixtures are chosen as the raw material and reaction medium, respectively. This molten-salt flux scheme

significantly improves the nanowire yield while maintaining high crystal quality and illustrates the feasibility of large-scale production of semiconductor nanowires. We additionally demonstrate that this method allows for incorporation of various transition-metal (TM) dopants into the TiO₂ lattice by introducing the corresponding TM salt as a dopant source. The homogeneity of the dopant speciation exhibits simultaneous benefits in both the optical properties and photocatalytic response of the TiO₂ nanowires.

In a typical synthesis, the present molten-salt flux method involves a blended mixture of TiO₂ nanoparticles, NaCl, and Na₂HPO₄, which is heated above the melting point of the salt mixture to achieve a large-scale synthesis of TiO₂ nanowires with a yield of about 99% (Figure 1a). X-ray diffraction (XRD) collected under a synchrotron radiation light source ($\lambda = 0.7749 \text{ \AA}$) shows the absence of any peaks other than that for the tetragonal rutile phase of TiO₂ (Figure 1b). Scanning electron microscopy (SEM) confirms the 1D nanowire morphology and reveals both uniform diameters of 100 nm and variable lengths from 5 to 40 μm , resulting in exceptionally large aspect ratios of up to 400 (Figure 1c,d). A representative transmission electron microscopy (TEM) image and diffraction pattern (Figure 1e) confirm that the nanowires are grown along the [001] direction and bounded by four {100} facets on the side wall, as evidenced by the sharp selected area electron diffraction (SAED) patterns examined along the [100] zone axis. The end tips, however, consist of four {011} facets focused to a point, where the tip angle matches nearly to the theoretical value of 113.88° (along the [100] zone axis). Examination of individual nanowire with high-resolution (HR) TEM shows that they are completely crystalline along their entire lengths (Figure 1f). Lattice fringes with interplanar spacings $d_{100} = 4.5 \pm 0.2 \text{ \AA}$ and $d_{001} = 2.9 \pm 0.1 \text{ \AA}$ are measured, consistent with the rutile crystal structure.

To investigate the nanowire formation mechanism, aliquoted products were examined *ex situ*. When the reaction was heated above 600 °C for more than 2 min, the percentage of anatase diffraction in the product was reduced compared to that in the unheated mixture of P25 nanoparticles, NaCl, and Na₂HPO₄ (Supporting Information, Figure S1 and S2). Concurrently, a new phase of monoclinic tetrasodium titanium nonaoxodiphosphate (Na₄TiP₂O₉) was observed.²¹ After 8 min of heating at 825 °C, the formation of the Na₄TiP₂O₉ intermediate plays a

Received: April 18, 2013

Published: July 1, 2013

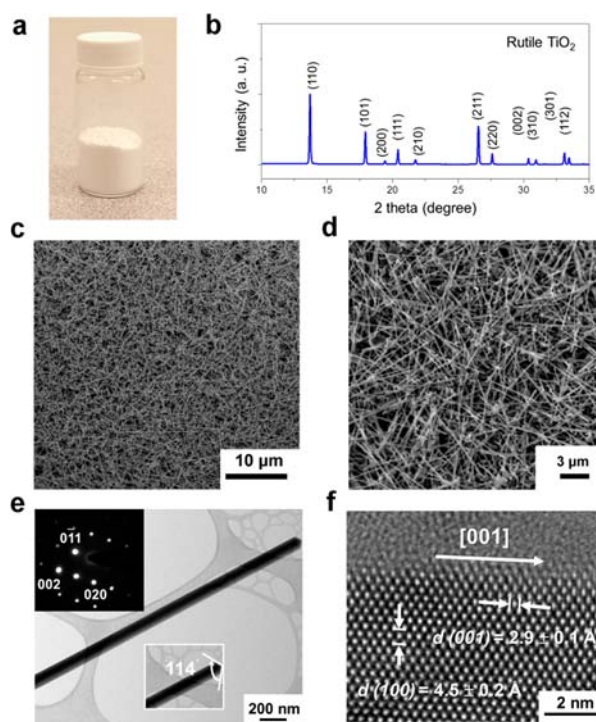


Figure 1. (a) Photograph of rutile TiO_2 nanowires. (b) XRD pattern of as-prepared TiO_2 nanowires. (c,d) SEM images of rutile TiO_2 nanowires. (e) TEM image of a single TiO_2 nanowire examined along the $[100]$ zone axis; insets show the corresponding SAED pattern and tip angle. (f) HRTEM image of a single TiO_2 nanowire.

critical role for rutile nanowire growth, as evidenced by the necessity of its formation to produce TiO_2 nanowires. Attempts using only NaCl or Na_2HPO_4 resulted in only rutile TiO_2 particles (Figure S3). A mixture of NaCl (80 wt%) and Na_2HPO_4 (20 wt%) achieved the lowest eutectic temperature and is shown to be the eutectic composition with the present reaction temperature (825 °C) according to the phase diagram,¹⁹ indicating that the molten environment maximizes the solubility and diffusivity of the reactant.

In addition to the influence of the salt mixture, variations of the reactant phase yielded controllable differences in the products. Anatase, the metastable phase of TiO_2 , readily reacts with $\text{Na}_4\text{P}_2\text{O}_7$ to form $\text{Na}_4\text{TiP}_2\text{O}_9$ at temperatures above 600 °C,²² while the thermodynamically stable rutile phase does not form this intermediate under the present condition. Consequently, pure anatase particles could be used as the titanium source to synthesize rutile nanowires as well (Figure S4); however, rutile nanowires synthesized from pure anatase particles have broader size distributions, suggesting that the synthesis of rutile nanowires is optimally performed through P25 nanoparticles containing both anatase and rutile phases, wherein they serve dual roles as both rutile seeds and TiO_2 nutrients. Anisotropic crystal growth of nanowires along the rutile c -axis results from lower solid–liquid interfacial energy and free energy minimization for growth occurring parallel to the $[001]$ direction.²³ The (011) facets observed at the tips of the nanowires work in concert with the (100) facet along the nanowire length to minimize the total surface energy, resulting in the formation of rutile nanowires with rectangular cross sections.²⁴

In addition to the large yield of single-crystalline nanowires, this synthetic scheme also allows for the introduction of TM

dopants. Historically, a variety of TMs have been explored as dopants in modifying the electronic structure of TiO_2 to improve its visible-light photocatalytic activity.^{25–28} Because of the interaction between the t_{2g} state of TM dopants and Ti atoms, TM doping could create an additionally occupied state in the bandgap of TiO_2 .²⁵ Here, through the introduction of TM dopants such as V, Cr, Mn, Fe, Co, Nb, Mo, and Rh during the molten-salt synthesis, the as-prepared 2% TM-doped TiO_2 nanowires (Figure S5) exhibit a variety of colors, departing from the white color of the undoped product. For instance, Rh-doped samples show a deep brown color resulting from strong absorption in the visible region (Figure 2). Consequently, the

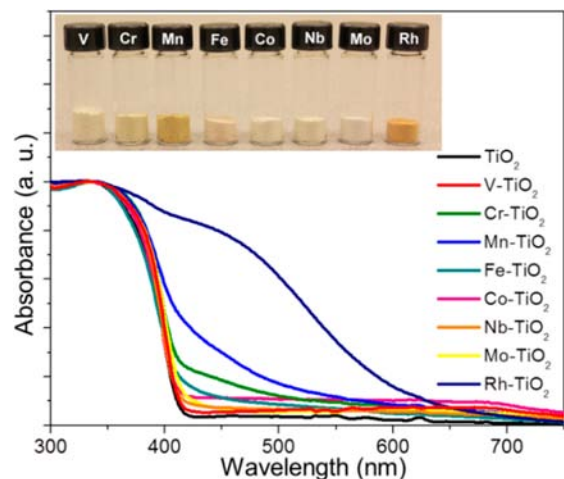


Figure 2. Photograph of various TM-doped TiO_2 nanowires and UV/vis spectra of various TM-doped TiO_2 nanowires.

light absorption edge of TM-doped TiO_2 nanowires extends from ultraviolet to visible, increasing the overlap between light absorption and the solar spectrum, thereby widening the range of sunlight that is able to be captured to generate carriers for photocatalytic reactions.

Since the photocatalytic properties of TM-doped TiO_2 nanowires can be strongly affected by the dopant speciation and position, XRD via synchrotron radiation was used to confirm that only the tetragonal rutile phase of TiO_2 exists in the doped samples (Figure 3a). This indicates that the optical variation can be attributed to the metal doping rather than the formation of undesired phases that may have been created as a result of adding dopant precursors to the reaction mixture. In order to probe short-range structure, extended X-ray absorption fine structure (EXAFS) spectra were collected for specific nearest-neighbor interatomic distances and coordination numbers (CNs).²⁹ Rutile has a tetragonal crystal structure, in which each Ti atom is surrounded by six O atoms in octahedral coordination, with two distinct bond lengths of 1.947 and 1.981 Å (Figure 3b). Correspondingly, three major peaks were present in the Fourier transforms (FTs) of the EXAFS data (Figure 3c). The first peak, at ~ 1.8 Å, of the FT EXAFS signal (first shell) obtained after phase correction is due to both families of O atoms. The second peak, at ~ 2.7 Å, of the FT is assigned to single scattering by Ti–Ti atoms occupying the centers of contiguous rectangular prisms (second shell), while the third peak, at ~ 3.4 Å, is in part to the eight Ti atoms occupying the vertices of the prism and in part to multiple scattering contributions from both Ti and O atoms (third shell). The second shell exhibits a significant change in both

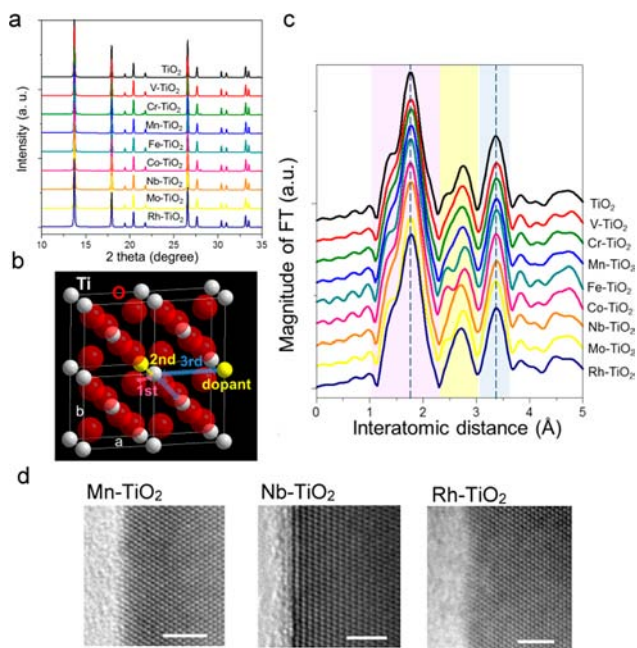


Figure 3. (a) XRD patterns of TM-doped TiO₂ nanowires, showing that there were no impurities forming in various dopants samples. (b) Rutile structure of TiO₂ and scattering shell modes around the Ti atom. (c) FT EXAFS spectra of various TM-doped samples. (d) HRTEM images of the rutile TiO₂ nanowires doped with Mn, Nb, and Rh (scale bar, 2 nm).

position and shape in various TM doping, revealing that the TM atoms substitute for Ti atoms at the same site around Ti atoms. Since the first shell was due to a single scattering of O atoms, and several multiple scatterings were involved in the third shell, these two shells give no additional information about the dopant position. Therefore, only the second shell was refined to extract quantitative structural parameters (Table S1). The Ti–Ti contribution at a distance of 3.01 Å for rutile TiO₂ nanowires and the CN around 1.93 is consistent with the bulk value for rutile TiO₂ (JCPDS file no. 88-1175). With regard to the TM doping, considerable contributions from the single scattering of TMs around Ti atoms were present in various cases of doped TiO₂ samples, revealing the TM atoms significantly exist around absorbing Ti atoms. Although the CN for the Ti–TM path cannot precisely reflect the doping amount in rutile crystal due to the low concentration of dopants (2%), this result still demonstrates the effectiveness of doping with TM in the present molten-salt method. HRTEM images of TM-doped TiO₂ nanowires further demonstrate that neither crystal defects nor other phases can be observed (Figure 3d). Furthermore, this synthetic route enables doping to occur before the subsurface layer begins to suffer from phase transformation and degradation, which is a common problem with diffusion-based, post-growth methods. *In situ* dopant incorporation allows for homogeneous dopant distributions, which can exhibit higher charge carrier mobility and higher visible-light absorbance than those of surface doping.²⁵

To examine the transport and photoelectrochemical properties, nanowire electrodes were fabricated by drop-casting nanowires onto FTO substrates. From the slopes of the Mott–Schottky plots (Figures 4a and S6), carrier densities of undoped and 2% Nb-doped TiO₂ nanowires were estimated to be $\sim 10^{15}$ and $\sim 10^{21}$ cm⁻³, respectively, using the following relation: $N_d = (2/e_0\epsilon\epsilon_0)[d(1/C^2)/dV]^{-1}$, where e_0 is the

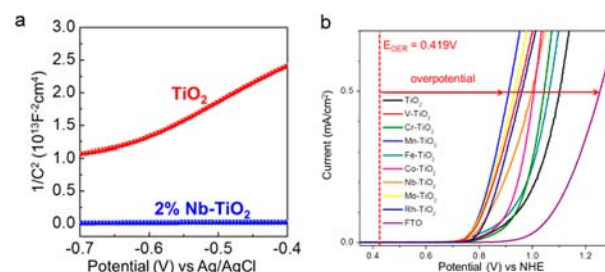


Figure 4. (a) Mott–Schottky plot of a TiO₂ and 2% Nb-TiO₂ nanowire electrode measured at 500 Hz. (b) Overpotential measurement for OER using FTO and TiO₂ nanowire with/without TM doping of electrodes in basic solutions. Dashed vertical lines represent the thermodynamic redox potential for water oxidation at pH ~ 13.6 .

electron charge, ϵ is the rutile TiO₂ dielectric constant ($\epsilon = 86$),³⁰ ϵ_0 is the vacuum permittivity, and N_d is the donor density.³¹ The positive slope indicates n-type behavior of the rutile nanowires. The low carrier density of the undoped sample reflects the high crystalline quality of the rutile nanowires, which is a result of the high temperature used in the molten-salt synthesis.

Dopant incorporation not only allows for flexibility to tune the carrier concentration of TiO₂ but also beneficially affects its photocatalytic performance. It is well-known that TiO₂ can be used as a photocatalyst for the photoelectrolysis of water.³² However, the large overpotential for the oxygen evolution reaction (OER) to occur commonly limits its performance. However, the introduction of TM dopants uniformly into the TiO₂ lattice causes substantial decreases in the overpotential (Figure 4b), where the overpotentials are compared in a specific current density of 0.5 mA/cm². Since the OER overpotential is affected by the binding energy with intermediates such as O*, HO*, and HOO*, TM dopants can lead to lower overpotentials due to stronger interactions of the adsorbed species on the surface.³³ We obtained an overpotential of 0.488 V on 2% Mn-doped TiO₂ nanowires, which represents a $\sim 28\%$ decrease in overpotential relative to that of pristine rutile TiO₂ (Table 1), indicating that TM substitutions on TiO₂ crystal are able to alter the adsorption energy of reaction intermediates for OER in spite of the low quantity of dopant. Several theoretical predictions of overpotentials are listed in Table 1 for comparison, in which 6.25% Mn doped on a rutile TiO₂ single crystal exhibited a 48% decrease in overpotential. While this prediction is greater than

Table 1. Experimental Overpotential Associated with OER on TM-Doped TiO₂ Nanowires and Theoretical Calculation from TM-Doped Rutile TiO₂ Single Crystal

sample, 2% dopant	overpotential (V)	
	exptl, at 0.5 mA/cm ²	calcd, 6.25% dopant ³²
FTO	0.836	–
TiO ₂	0.681	1.3
V-TiO ₂	0.529	–
Cr-TiO ₂	0.623	–
Mn-TiO ₂	0.488	0.69
Fe-TiO ₂	0.644	–
Co-TiO ₂	0.586	–
Nb-TiO ₂	0.578	0.76
Mo-TiO ₂	0.514	0.74
Rh-TiO ₂	0.539	–

the measured reduction, this discrepancy might be due to a lower substitution ratio than that used in theoretical simulation. Although the determination of overpotential was experimentally current-dependent, the absolute values from prediction and experiment cannot be directly compared, but the trends can be compared relatively. We observed OER overpotential of various TM doping in the sequence Mn-TiO₂ < Mo-TiO₂ < Nb-TiO₂ < TiO₂, which follows the same trend as theoretical simulations, even with the difference in dopant concentration.³³

In summary, the molten-salt flux method allows for the synthesis of TiO₂ nanomaterials in large quantities and has the potential for mass production in future nanomaterial production. Transition-metal doping allows for tunable optical absorption and tailored capture of visible light, as well as decreases of the OER overpotential in the electrolysis of water, which could benefit TiO₂ photoactivity, especially for water oxidation, and considerably suppress this kinetic loss of overpotential. Considering the advantage and versatility offered by this molten-salt method, the findings here can have an important impact in making large-scale, tunable, and durable synthesis of various 1D materials a reality.

■ ASSOCIATED CONTENT

📄 Supporting Information

Experimental details, Figure S1–S6, and Table S1. This material is available free of charge via the Internet at <http://pubs.acs.org>.

■ AUTHOR INFORMATION

Corresponding Author

p_yang@berkeley.edu

Author Contributions

[‡]B.L. and H.M.C. contributed equally.

Notes

The authors declare no competing financial interest.

■ ACKNOWLEDGMENTS

This work was supported by the Director, Office of Science, Office of Basic Energy Sciences, Materials Sciences and Engineering Division, U.S. Department of Energy under Contract No. DE-AC02-05CH11231.

■ REFERENCES

- (1) Xia, Y. N.; Yang, P. D.; Sun, Y. G.; Wu, Y. Y.; Mayers, B.; Gates, B.; Yin, Y. D.; Kim, F.; Yan, Y. Q. *Adv. Mater.* **2003**, *15*, 353.
- (2) Law, M.; Goldberger, J.; Yang, P. D. *Annu. Rev. Mater. Res.* **2004**, *34*, 83.
- (3) Hochbaum, A. I.; Yang, P. D. *Chem. Rev.* **2010**, *110*, S27.
- (4) Huang, M. H.; Mao, S.; Feick, H.; Yan, H. Q.; Wu, Y. Y.; Kind, H.; Weber, E.; Russo, R.; Yang, P. D. *Science* **2001**, *292*, 1897.
- (5) Law, M.; Greene, L. E.; Johnson, J. C.; Saykally, R.; Yang, P. D. *Nat. Mater.* **2005**, *4*, 455.
- (6) Law, M.; Sirbully, D. J.; Johnson, J. C.; Goldberger, J.; Saykally, R. J.; Yang, P. D. *Science* **2004**, *305*, 1269.
- (7) Tang, J. Y.; Huo, Z. Y.; Brittman, S.; Gao, H. W.; Yang, P. D. *Nanotechnol.* **2011**, *6*, 568.
- (8) Cui, Y.; Wei, Q. Q.; Park, H. K.; Lieber, C. M. *Science* **2001**, *293*, 1289.
- (9) Chan, C. K.; Peng, H. L.; Liu, G.; McIlwrath, K.; Zhang, X. F.; Huggins, R. A.; Cui, Y. *Nat. Nanotechnol.* **2008**, *3*, 31.
- (10) Morales, A. M.; Lieber, C. M. *Science* **1998**, *279*, 208.
- (11) Wu, Y. Y.; Yang, P. D. *J. Am. Chem. Soc.* **2001**, *123*, 3165.
- (12) Yang, P. D.; Lieber, C. M. *Science* **1996**, *273*, 1836.

- (13) Trentler, T. J.; Hickman, K. M.; Goel, S. C.; Viano, A. M.; Gibbons, P. C.; Buhro, W. E. *Science* **1995**, *270*, 1791.
- (14) Liu, B.; Aydil, E. S. *J. Am. Chem. Soc.* **2009**, *131*, 3985.
- (15) Morin, S. A.; Bierman, M. J.; Tong, J.; Jin, S. *Science* **2010**, *328*, 476.
- (16) Greene, L. E.; Law, M.; Goldberger, J.; Kim, F.; Johnson, J. C.; Zhang, Y. F.; Saykally, R. J.; Yang, P. D. *Angew. Chem., Int. Ed.* **2003**, *42*, 3031.
- (17) Yang, P. D.; Yan, R. X.; Fardy, M. *Nano Lett.* **2010**, *10*, 1529.
- (18) Arendt, R. H.; Rosolowski, J. H.; Szymaszek, J. W. *Mater. Res. Bull.* **1979**, *14*, 703.
- (19) Roy, B.; Ahrenkiel, S. P.; Fuierer, P. A. *J. Am. Ceram. Soc.* **2008**, *91*, 2455.
- (20) Roy, B.; Fuierer, P. A. *J. Am. Ceram. Soc.* **2010**, *93*, 436.
- (21) Bolotina, N. B.; Maximov, B. A.; Petricek, V.; Simonov, V. I. *Kristallografiya* **1995**, *40*, 611.
- (22) Kabbour, H.; Coillot, D.; Colmont, M.; Masquelier, C.; Mentre, O. *J. Am. Chem. Soc.* **2011**, *133*, 11900.
- (23) Oliver, P. M.; Watson, G. W.; Kelsey, E. T.; Parker, S. C. *J. Mater. Chem.* **1997**, *7*, 563.
- (24) Ramamoorthy, M.; Vanderbilt, D.; Kingsmith, R. D. *Phys. Rev. B* **1994**, *49*, 16721.
- (25) Liu, G.; Wang, L.; Yang, H. G.; Cheng, H.-M.; Lu, G. Q. *J. Mater. Chem.* **2010**, *20*, 831.
- (26) Bak, T.; Nowotny, J.; Rekas, M.; Sorrell, C. C. *Int. J. Hydrogen Energy* **2002**, *27*, 991.
- (27) Janisch, R.; Gopal, P.; Spaldin, N. A. *J. Phys.: Condens. Matter* **2005**, *17*, R657.
- (28) Wang, Y.; Hao, Y.; Cheng, H.; Ma, J.; Xu, B.; Li, W.; Cai, S. *J. Mater. Sci.* **1999**, *34*, 2773.
- (29) Iwasawa, Y. *X-ray Absorption Fine Structure for Catalysts and Surfaces*; World Scientific: Singapore, 1996.
- (30) Parker, R. A. *Phys. Rev.* **1961**, *124*, 1719.
- (31) Furubayashi, Y.; Hitosugi, T.; Yamamoto, Y.; Inaba, K.; Kinoda, G.; Hirose, Y.; Shimada, T.; Hasegawa, T. *Appl. Phys. Lett.* **2005**, *86*, 252101.
- (32) Fujishima, A.; Honda, K. *Nature* **1972**, *238*, 37.
- (33) Garcia-Mota, M.; Vojvodic, A.; Metiu, H.; Man, I. C.; Su, H. Y.; Rossmeisl, J.; Nørskov, J. K. *Chemcatchem* **2011**, *3*, 1607.